Sub-Doppler Saturation Spectroscopy of HCN up to 1 THz and Detection of $J = 3 \rightarrow 2$ ($4 \rightarrow 3$) Emission from TMC1

Volker Ahrens, Frank Lewen, Shuro Takano*, Gisbert Winnewisser, Štepán Urban[a], A. A. Negirev[b], and A. N. Koroliev[b]

I. Physikalisches Institut der Universität zu Köln, D-50937 Köln

[a] J. Heyrovský Institute, Academy of Sciences of the Czech Republic, 182 23 Praha 8, Czech Republic

[b] ISTOK, Research and Production Company, Fryazino, Moscow Region, Russia

* Present address: Nobeyama Radio Observatory, Nobeyama, Minamimaki, Minamisaku, Nagano, 384-1305, Japan

Reprint requests to Prof. G. W.; E-mail: winnewisser@ph1.uni-koeln.de

Z. Naturforsch. **57 a,** 669–681 (2002); received April 8, 2002

Very high-resolution ($\sim$ 30 kHz) and very precise ($\pm$2 kHz) saturation dip and crossover dip measurements are reported for HCN. Nine consecutive rotational transitions of the vibrational ground state were recorded, covering the rotational spectrum up to the $J = 11 \leftarrow 10$ transition at 975 GHz. Commencing the saturation dip measurements with the $J = 3 \leftarrow 2$ transition located at 265 886.4 MHz, all rotational transitions were measured up to $J = 11 \leftarrow 10$ ($\Delta F = 1$), positioned at a center frequency of 974 487.2 MHz. It has become possible to resolve the hyperfine structure of every rotational transition to varying degrees. Transitions obeying the selection rules $\Delta J = 1$, $\Delta F = 0$ are have been resolved, those obeying the selection rules $J = 1$, $F = 1$ are only resolved for transitions lower than the $J = 6 \leftarrow 5$ transition.

These new experimental saturation dip data, together with the molecular beam maser emission data of the $J = 1 \rightarrow 0$ and $J = 2 \rightarrow 1$ transitions reported by De Lucia and Gordy, (Phys. Rev. **187**, 58 (1969)), and the recent terahertz measurements performed in this laboratory up to J = 22-21 at 1.946 THz (Maiwald et al., J. Mol. Spectrosc. **202**, 166 (2000)), were subjected to a least squares analysis which yielded a highly precise set of molecular constants for the ground state of HCN: B = 44 315.974 970 (156) MHz, D = 0.087 216 35 (169) MHz, H = 0.086 96 (242) Hz; eQq = –4.709 03 (162) MHz, eQq_J = 0.244 (88) Hz, C_N = 10.09 (38) kHz, C_{NJ} = –0.0143 (86) mHz.

Two constants, the hydrogen *spin*-rotation, C_H = –4.35 (5) kHz, and the *spin-spin* interaction between the proton and nitrogen nucleus, S_{NH} = 0.154 (3) kHz, can not be determined from the saturation dip measurements and have been taken from Ebenstein and Muenter, J. Chem. Phys. **80**, 3989 (1984). There also a value for the ground state permanent electric dipole moment (in Debye's) is given, which we quote for completeness: $\langle\mu\rangle_{000}$ = 2.985 188 (3) D.

We also report the discovery of the $J = 3 \rightarrow 2$ and $J = 4 \rightarrow 3$ ground state rotational transitions of HCN in the dark, cold molecular cloud TMC1 by using the KOSMA 3m-Submillimeter Telescope located in the central Swiss Alps. For the $J = 3 \rightarrow 2$ transition the hyperfine splitting has partly been resolved. The intensities of the hyperfine components are anomalous, and they are not in thermodynamic equilibrium.

Key words: Sub-Doppler Measurement; Saturation Spectroscopy; Rotational Spectrum; Submillimeter Transitions; Interstellar Molecular Spectroscopy; Dark Clouds.

Introduction

Since the first observation of the rotational transition $J = 1 \leftarrow 0$ by Gordy and collaborators [1, 2] in 1949, hydrogen cyanide, HCN, has been the subject of many detailed investigations. The main goal of these early publications was to establish, first of all, a reliable experimental data base and consequently to derive from these data accurate molecular parameters for HCN and its various isotopomers in their ground and vibrationally excited states.

As a linear triatomic molecule, HCN displays a fairly simple pure rotational spectrum that consists of an R branch for the vibrational ground state. In addi-

tion to the regular R branch $\Delta J = 1$ millimeter- and sub-millimeter wave transitions, Q branch $\Delta J = 0$ transitions occur between vibrationally excited degenerate state levels that are connected by *l*-type resonance matrix elements. The latter transitions are also called "direct *l*-type transitions" and have been observed in the laboratory and in interstellar space. The HCN rotational spectra display many features that are also of interest from a theoretical point of view, such as comparison with *ab initio* calculations, or the large amplitude motion aspect of the bending vibration.

Since the discovery of HCN in various types of interstellar clouds [3, 4], this molecule has also become of high astrophysical interest, both in the ground and in excited bending states. Especially the medium J rotational transitions of the R branch in the vibrational ground state have become good tracers of high-density interstellar gas [5], whereas circumstellar HCN maser action has been discovered in various vibrationally excited levels [6]. The direct *l*-type transitions have also been discovered in space [21]. Detailed references to the laboratory and the interstellar measurements reported before 1977 are found in the compilation made by Lovas [7]. Laboratory spectra for the less abundant isotopomers, particularly those with more than one substituted nucleus, have been reported in 1993 [8].

In this paper we display nine R branch transitions of the pure rotational spectrum of HCN recorded and measured in saturation dip spectroscopy. The Cologne terahertz spectrometer was operated in the sub-Doppler mode. It should be emphasized that this presentation is the first one ever and probably the most comprehensive to date to display every rotational transition of a molecule in sub-Doppler resolution up to 1 THz, with the aim to reveal as much of the underlying hyperfine structure as possible.

HCN Electric Quadrupole and Magnetic Hyperfine Structure

The nonspherical distribution of the positive nuclear charge of ^{14}N ($I_N = 1$) produces an electric nuclear quadrupole moment, which due to interaction with the negative electron field gives rise to a sizeable hyperfine structure (hfs). In addition, the nuclear spin of ^{14}N atom behaves as a microscopic magnet with a magnetic moment that interacts with the magnetic field produced by rotating charged particles (electrons and nuclei). This interaction, called nuclear spin rotation interaction, contributes to the electric quadrupole hyperfine structure. Although the expressions for the quadrupole energy and spin-rotation interaction for a single nucleus in a linear molecule is well understood, it seems at this point advantageous to shortly summarize the effect of the hyperfine interaction on the splitting of the rotational energy levels and its associated line pattern. With the exception of the $J = 0$ rotational level, each rotational state is split into a triplet due to the ^{14}N hyperfine interaction. The recorded sub-Doppler line pattern reflects this interaction for all transitions observed in this work.

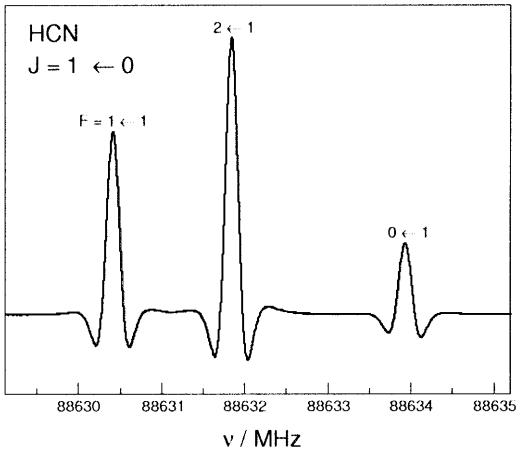

Fig. 1. The lowest rotational transition of HCN recorded with high signal to noise ratio. The spectrum has been recorded in Doppler resolution. The three hyperfine components have been measured and they agree within 1 kHz with the beam maser measurements of De Lucia and Gordy [9]. The Doppler limited spectrum yielded the following transition frequencies: F = 1-1 88 630.4157 MHz, F = 2-1 88 631.8483 MHz, F = 0-1 88 633.9342 MHz.

The nitrogen-^{14}N nucleus electric quadrupole interaction causes the lowest rotational transition J = 1-0 to be split into a hyperfine triplet, whereas six hyperfine components are expected for all higher rotational transitions. The spectral resolution reached by Doppler limited techniques is sufficient to fully resolve the triplet hyperfine splitting of the J = 1-0 transition (Fig. 1). However, the expected additional, very small hyperfine nuclear spin-spin splitting caused by the magnetic coupling between the nitrogen ^{14}N ($I_N = 1$) and hydrogen ($I_H = 1/2$) remained unresolved, even for sub-Doppler beam maser techniques [8].

According to the selection rules $\Delta J = 1$, $\Delta F = 0, \pm 1$, the hyperfine pattern of the J = 2-1 rotational

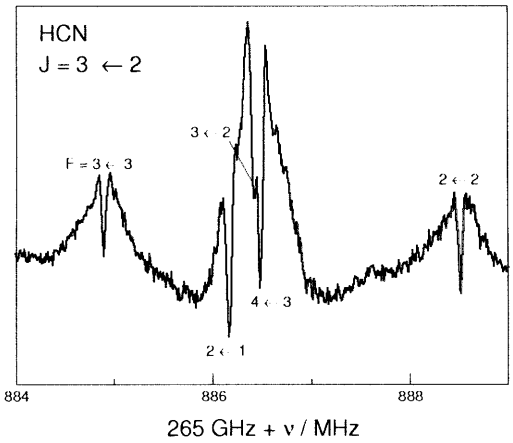

Fig. 2.1. The J = 3-2 rotational transition of HCN recorded in sub-Doppler resolution. The five expected saturation dips are identified. The background "baseline" traces the Doppler-profile. – Figures 2.1 - 2.9 portray consecutive rotational transitions of HCN in the vibrational ground state in sub-Doppler resolution.

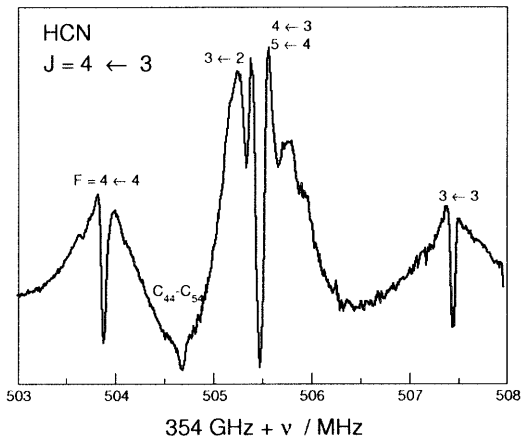

Fig. 2.2. Lamb dip spectrum of the J = 4-3 rotational transition depicts the three "inner" hyperfine components superimposed on the Doppler profile. In addition to the five absorption dips one crossover dip occurs, C_{44}-C_{54}, indicating that two Doppler profiles overlap (see text).

transition and all higher J rotational transitions consists of a hyperfine sextet. However, only five of the six components are usually observed, since the ΔF = –1 component carries only about 0.6% of the transition's total intensity, which is usually too weak to be resolved. In particular, this line is very difficult to measure, since it is located in close vicinity to the dominating ΔF = +1 components. This statement holds true for all measurements reported here, in the sense that the ΔF = –1 hyperfine component has not been observed for any rotational transition recorded in this work. Thus each rotational transition displays a similar hyperfine pattern, consisting of three very closely spaced hyperfine components (ΔJ = 1, ΔF = 1), which carry most of the rotational transition's total intensity. This "inner" triplet of hyperfine components is accompanied by two somewhat more widely spaced components, i. e. $\Delta J = 1, \Delta F = 0$. However, each of them carries only a small fraction of the intensity of the entire transition, i. e. within a factor of 2 the strength of the transition is proportional to $\sim 1/J^2$. One of these "outer" hyperfine components is positioned on the low, the other on the high frequency side relative to the "inner" hyperfine triplet.

Saturation Measurements

All ground state rotational transitions up to J = 11-10 of HCN have now been recorded in sub-Doppler resolution and are displayed in a sequence of nine recordings (Figs. 2.1 - 2.9). The hyperfine pattern of the two lowest rotational transitions has been fully resolved by millimeter-wave molecular beam maser techniques [9] developed by De Lucia and Gordy. The other nine rotational transitions are presented here in a sequence of figures, intended to demonstrate the occurrence of saturation dips and crossover dips. These experimental data are presented

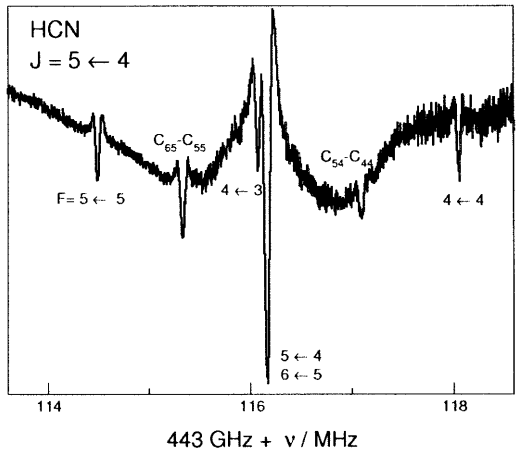

Fig. 2.3. The J = 5-4 transition in sub-Doppler resolution displaying the inner three components as two barely resolved saturation dips together with the two outer dips. In addition two crossover dips complete the detectable absorption dips.

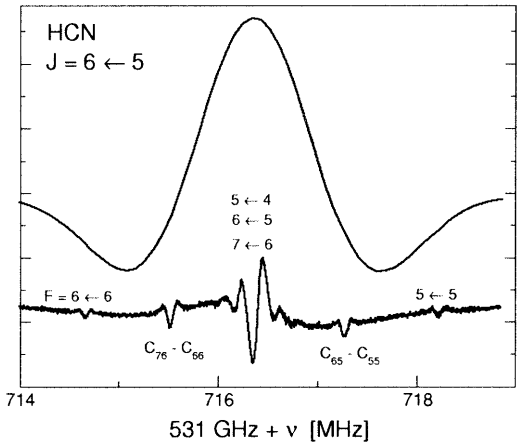

Fig. 2.4. A comparison between the Doppler profile (upper trace) of the $J = 6$-5 rotational transition and the same scan in sub-Doppler resolution (lower trace). The three "inner" hyperfine components have merged to the point where it is not possible to separate them even with saturation dip spectroscopy.

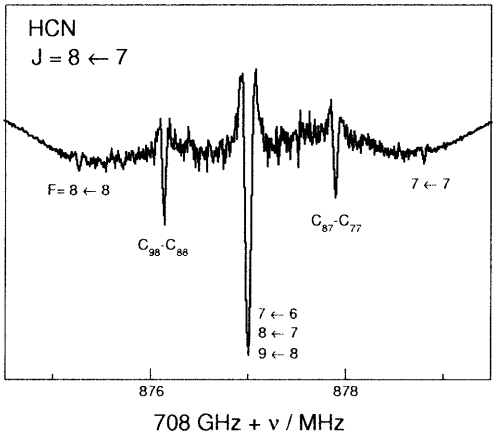

Fig. 2.6. The J = 8-7 transition in sub-Doppler resolution. Here one is left with one dip for the "inner three" hf-components, with two clearly detectable crossover dips and barely visible two outer hf-components. In cases like that, the crossover dips can be used to measure the location of the outer hf-components of the rotational transition.

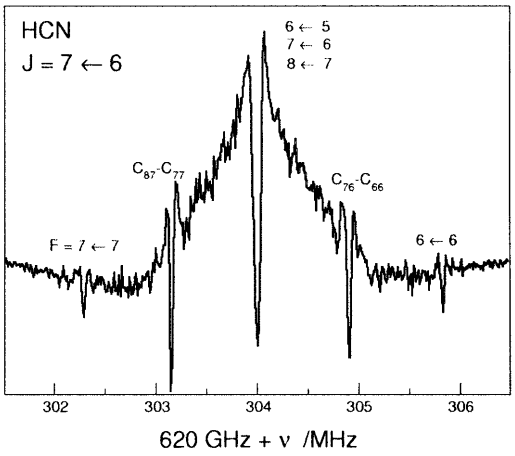

Fig. 2.5. The J = 7-6 transition in sub-Doppler resolution, where the outer two hfs-components just show up. It should be noted that the two crossover dips exhibit good signal / noise ratio.

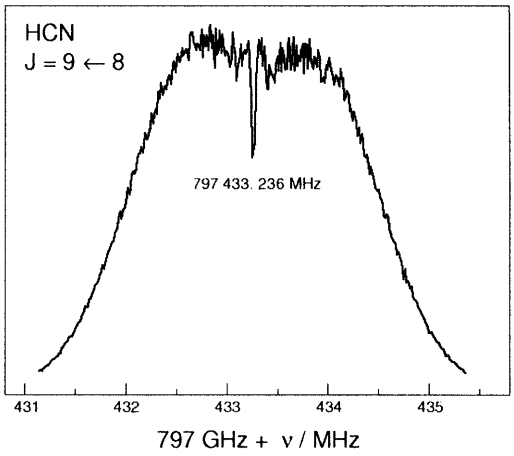

Fig. 2.7. The central dip caused by the "inner three" hf-components of the J = 9-8 rotational transition.

in two blocks of recordings, i. e. Figs. 2.1 - 2.4 and Figs. 2.5 - 2.9.

In our saturation dip measurements of HCN, the hyperfine pattern is best borne out by the J = 3-2 transition. The achieved resolving power by the saturation dip technique was just sufficient to barely separate the "inner" triplet of hyperfine components, i. e. ($\Delta J = 1$, $\Delta F = 1$), as shown in Fig. 2.1. However, as one moves to consecutively higher J rotational transitions, small but significant changes occur in the relative intensities and positions of each individual hyperfine component. As expected, the more intense components, i. e. the "inner" triplet of the hyperfine structure are those, for which $\Delta J = \Delta F = +1$, and for these the hyperfine structure decreases as J increases. For the two weaker "outer" components $\Delta J = 1$, $\Delta F = 0$ the change in quadrupolar energy is larger and the splitting decreases very slightly as J increases. Their relative intensity decreases with increasing J values (as $\sim 1/J^2$). This behaviour can

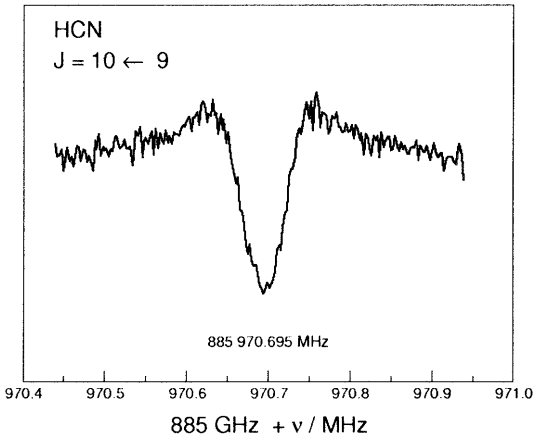

Fig. 2.8. Same as 2.7, but J = 10-9.

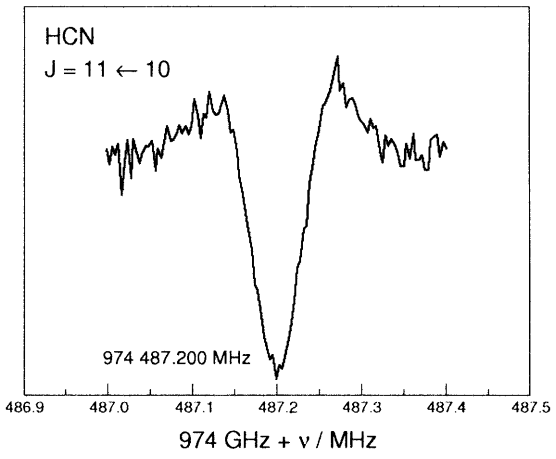

Fig. 2.9. Same as 2.7, but J = 11-10.

be studied advantageously by saturation dip spectroscopy as displayed in Fig. 2.2, where we present a recording of the J = 4-3 transition, the inner triplet of which is barely resolved. For the next higher rotational transition, J = 5-4, two of the three hyperfine components, i. e. F = 5-4 and 6-5 have merged, whereas the third hyperfine component, F = 4-3, can still be resolved, as depicted in Figure 2.3. In comparing Fig. 2.1 with Fig. 2.2 and Fig. 2.3, one notices that the J = 4-3 and J = 5-4 recordings display in addition to the expected five Lamb dips, corresponding to the center of the lines, two more, but very weak dips. These additional two dips are called "crossover" dips, and their occurrence will be discussed below.

Further details and references on earlier saturation dip spectroscopy in the submillimeter wave region carried out in the Cologne laboratory are found in [10 - 12].

Saturation and Crossover Dips

Power saturation of the purely Doppler broadened line profile produces a narrow (~40 kHz) dip at the center of the transition. The theory of saturation dips [13] has been worked out by using the density matrix formulation [14 - 16]. The full linewidth at half maxima $\Delta_{1/2}$ (FWHM) of the Lamb dip is limited by the natural life time broadening:

$$\Delta_{1/2} = \frac{\gamma}{2\pi} = (2\pi\tau_{sp})^{-1}, \quad (1)$$

where τ_{sp} is the spontaneous lifetime. The intensity of the dip is proportional to $(\mu_{12}E)^4$, where E stands for the intensity of the monochromatic electromagnetic field and μ_{12} is the matrix element of the corresponding hyperfine transition moment.

Figure 2.4 presents for the J = 6-5 transition a comparison between the Doppler-limited and Doppler-free spectrum. The Doppler limited line profile shows no indication of any possible hyperfine structure. In the sub-Doppler spectrum the Lamb dips associated with the unresolved "inner" triplet (ΔJ = 1, ΔF = +1; F = 5-4, 6-5, 7-6) of hyperfine components have merged to form one strong central dip. In addition, two fairly weak, but clearly resolved outer hyperfine components (F = 5-5, 6-6) are detected together with the appropriate crossover dips. The two outer hyperfine components and two of the inner ones, share one common level with each of the outer hfs components ΔJ = 1, ΔF = 0, as one can see in the appropriate energy level diagram displayed in Figure 3.

In addition to the Lamb dips, crossover dips can occur for any two lines which meet two conditions simultaneously: (i) they have to share one energy level in common and (ii) the level separation has to be within the Doppler width, which is the case for the HCN hfs-split rotational levels. For the J = 7 and 6 levels the two possible crossover dips are marked in Figure 3. Since the crossover dip occurs at exactly the average frequency of the pair of lines $(\nu_{12} + \nu_{13})/2$, they can be used additionally for the frequency determination of the hf component. We note that the crossover dip displays the same width as the normal saturation dips, its intensity being proportional to the

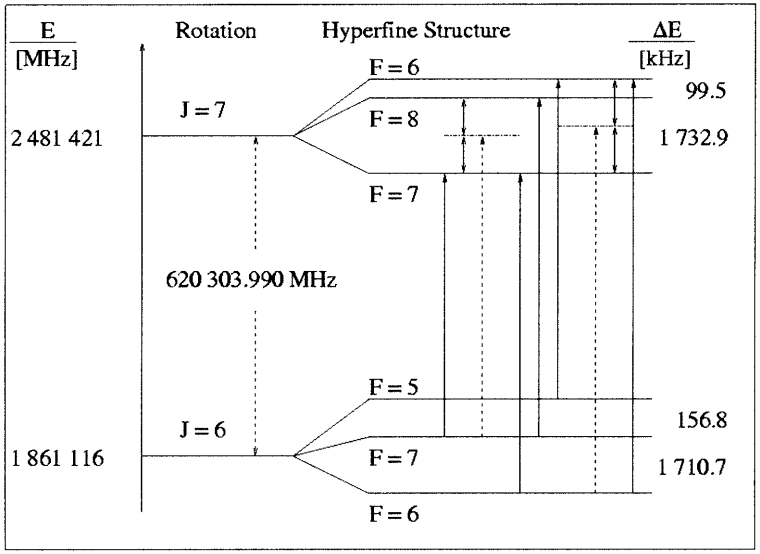

Fig. 3. Energy level scheme of the J = 7-6 transition and the expected five Lamb dips, together with the origin of the crossover dips.

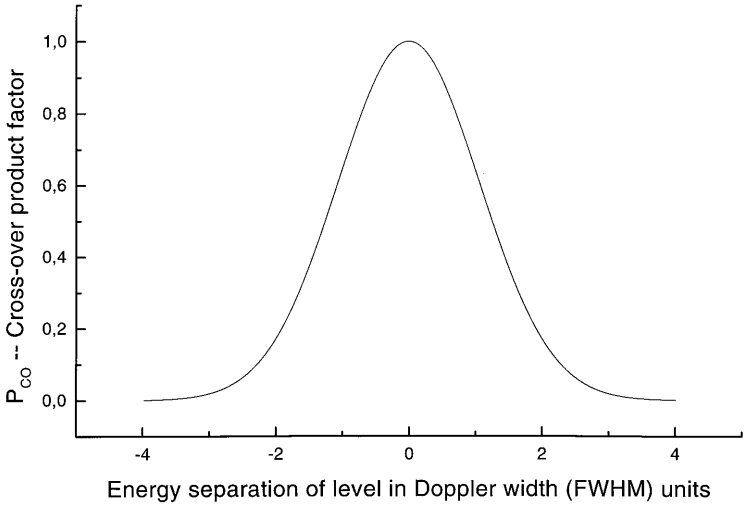

Fig. 4. The crossover product factor P_{CO} (see text) versus the energy separation of the level in units of Doppler widths.

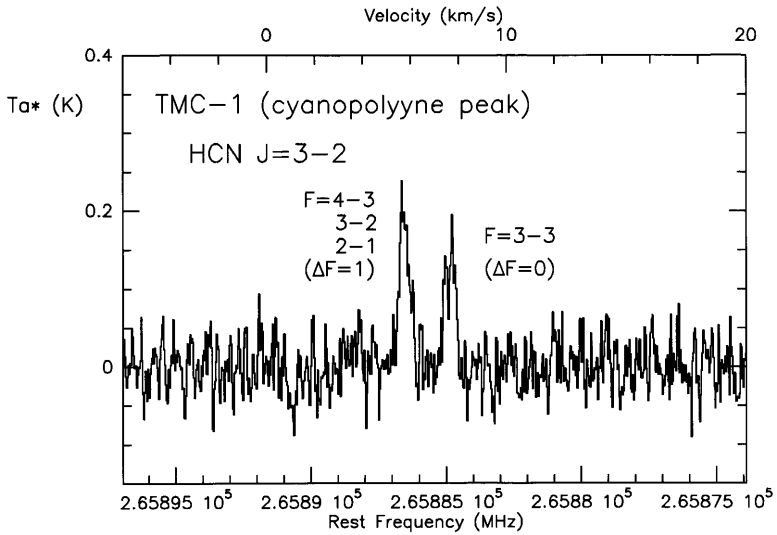

Fig. 5. The interstellar detection spectrum of the J = 3 → 2 transition of HCN towards the Taurus Molecular Cloud, TMC1-cyanopolyyne peak. It is clearly noted from the observed spectrum, that one of the outer hyperfine components, i. e. F = 2 → 2 is completely missing, while the other outer component F = 3 → 3 is almost as intense as the three center components.

product of the sqares of the two transition moments of the corresponding transitions sharing a common level (upper or lower):

$$I_{\mathrm{co}} \approx P_{\mathrm{CO}}\mu_{12}^2\mu_{13}^2E^4 = P_{CO}\mu_{\mathrm{R}}^2 f_{12}^2 f_{13}^2 E^4, \quad (2)$$

where μ_{R} is rotational transition moment, f_{ij} is the "hyperfine Hoenl-London" factor for the corresponding hyperfine component and P_{CO} is a dimensionless cross-over product factor expressing an overlap of the Doppler profile functions This factor can be written using the Doppler width (FWHM) $\Delta_{1/2}^{\mathrm{D}}$:

$$P_{\mathrm{CO}} = \exp\left[-2\ln 2(\nu_{12}-\nu_{13})^2/(\Delta_{1/2}^{\mathrm{D}})^2\right], \quad (3)$$

where $(\nu_{12}-\nu_{13})$ is the energy levels separation. The Doppler width (FWHM) can be calculated using the Maxwell distribution and for HCN at 295 K we get

$$\Delta_{1/2}^{\mathrm{D}} = \nu 7.15\times10^{-7}\cdot\sqrt{T/M} = \nu 2.36\times10^{-6}, \quad (4)$$

where ν is frequency of the corresponding crossover dip. The values of the overlap product factor are in interval 0-1 and can be expressed in Doppler units as it shows Figure 4. The crossover dips are marked in Fig. 2.3 and in all following ones by an upper case C with the appropriate hyperfine energy levels F as suffices. As an example, the two hyperfine transitions F = 7-6 and F = 6-6 share as common level J = 5, F = 6, and consequently the appropriate crossover dip carries the label C_{76}-C_{66} , where the energy separation between the levels J = 6, F = 6 and J = 6, F = 7 is about 1.71 MHz which is 1.34 $\Delta_{1/2}^{\mathrm{D}}$ of the corresponding Doppler width (1.25 MHz). It provides the value of the crossover-overlap factor P_{CO} of 0.45 (see Fig. 4). Accordingly, the only expected other crossover dip is C_{65}-C_{55}. For a comparison, the Doppler width $\Delta_{1/2}^{\mathrm{D}}$ of the J = 3-2 rotational transition at 265 886 MHz is about 0.63 MHz, the energy separation between J = 3, F = 3 and J = 3, F = 4 is about 2.55 $\Delta_{1/2}^{\mathrm{D}}$, and the corresponding value of the crossover-overlap factor P_{CO} is only 0.06 (see Fig. 1) and no cross-over dip has been observed.

Figures 2.5 - 2.9 illustrate the recordings of the remainder of the submillimeter wave HCN transitions commencing with the J = 7-6 rotational transition and ending with the J = 11-10 located at 974 487 MHz. For the three rotational transitions J = 9-8, 10-9, and 11-10 only a central dip has been observed, corresponding to the three "inner" hf-components.

Saturation Dip Measurement and Results

In Table 1 we have collected all power saturation dip sub-Doppler measurements carried out in this work together with the maser beam measurements provided by De Lucia and Gordy [9]. Since 1995, the time high power BWO-tubes made in Russia became available, we have performed saturation dip measurements up to 1 THz.

In the early 1990'ies the Wall came down separating the East from the West, and in its wake relations eased to the point that it became possible to introduce in the Cologne laboratories Russian made *b*ackward *w*ave *o*scillators (BWOs). Consequently, we developed the technique of phase-stabilisation [17, 24] for the BWOs up to about 1.3 THz. With this technique at hand, we could demonstrate their superiority by revealing the extremely high spectral purity of the tubes and their smooth broad frequency tunability.

The BWOs are produced by ISTOK, the Russian Research and Production Company, located in Fryazino, Moscow region. In collaboration with ISTOK several, specially developed high power-output BWOs have been used in the present work covering the entire frequency region from 260 GHz to 1.2 THz. Higher frequencies we have reached by frequency multiplication (see e. g. [18]).

Ground State Molecular Constants

The spectroscopic constants for HCN quoted by various authors are collected in Table 2. For comparison, we quote the molecular parameters given by DeLucia and Gordy [9], those recently obtained by Maiwald et al. [18], and the ones derived from the present saturation dip data only, together with a set of constants derived from selected molecular transitions considered to be most precisely measured. It is to be noted that the molecular parameters derived from the latter data set are extremely precise and we consider them presently to be the most reliable set of experimental molecular parameters for the ground state of HCN. It is revealing to compare in Table 2 the values of the rotational and centrifugal distortion constants B, D, and H in the vibrational ground state of either Maiwald et al. [18], or saturation dip data, with those derived by Maki [19] from FT-IR data only.

The most reliable set of molecular constants so far (column 2 in Table 2) has been derived in this work from a simultaneous fit of a selected set of high

Table 1. Sub-Doppler rotational spectrum of HCN[a].

J' F' J'' F''	ν_{exp}	σ	Diff	$^{R}I_{lin}$	$^{R}I_{sat}$	$^{A}I_{lin}$	$^{A}I_{sat}$
1 ⟵ 0	88631.6011	(0003)					
1 1 ← 0 1	88630.4157	(0010)	0.0018	33.38	25.81	0.16E-02	0.27E-05
1 2 ← 0 1	88631.8473	(0010)	0.0007	55.50	71.33	0.27E-02	0.73E-05
1 0 ← 0 1	88633.9360	(0010)	0.0008	11.12	2.86	0.54E-03	0.29E-06
2 ⟵ 1	177261.1090	(0006)					
2 2 ← 1 2	177259.6767	(0020)	0.0001	8.34	2.26	0.32E-02	0.10E-04
2 1 ← 1 0	177259.9233	(0020)	0.0016	11.11	4.01	0.42E-02	0.18E-04
2 2 ← 1 1	177261.1104	(0020)	0.0011	24.98	20.30	0.95E-02	0.90E-04
2 3 ← 1 2	177261.2232	(0020)	0.0035	46.69	70.91	0.18E-01	0.31E-03
2 1 ← 1 1	177263.4450	(0020)	0.0019	8.34	2.26	0.32E-02	0.10E-04
3 ⟵ 2	265886.4306	(0010)					
3 3 ← 2 3	265884.8828	(0020)	–0.0051	3.71	0.43	0.45E-02	0.20E-04
3 2 ← 2 1	265886.1660	(0300)	–0.0192	19.98	12.62	0.24E-01	0.59E-03
3 3 ← 2 2	265886.4240	(0400)	–0.0070	29.64	27.78	0.36E-01	0.13E-02
3 4 ← 2 3	265886.4870	(0200)	–0.0093	42.85	58.06	0.52E-01	0.27E-02
3 2 ← 2 2	265888.5164	(0020)	–0.0026	3.71	0.43	0.45E-02	0.20E-04
4 ⟵ 3	354505.4729	(0013)					
4 4 ← 3 4	354503.8790	(0050)	0.0138	2.08	0.13	0.56E-02	0.31E-04
4 4/5 - 3 4/4	354504.6780	(0300)	–0.0135	—	0.47	—	0.11E-03
4 3 ← 3 2	354505.3390	(0400)	–0.0234	23.78	17.39	0.64E-01	0.40E-02
4 4 ← 3 3	354505.4880	(0400)	0.0145	31.20	29.93	0.83E-01	0.69E-02
4 5 ← 3 4	354505.4880	(0400)	–0.0299	40.82	51.24	0.11E+00	0.12E-01
4 3 ← 3 3	354507.4469	(0050)	–0.0035	2.08	0.13	0.56E-02	0.31E-04
5 ⟵ 4	443116.1432	(0018)					
5 5 ← 4 5	443114.4920	(0040)	0.0008	1.33	0.05	0.63E-02	0.40E-04
5 5/6 - 4 5/5	443115.3325	(0020)	–0.0015	—	0.51	—	0.37E-03
5 4 ← 4 3	443116.0771	(0100)	–0.0008	26.02	20.53	0.12E+00	0.15E-01
5 5 ← 4 4	443116.1690	(0100)	0.0251	31.95	30.94	0.15E+00	0.23E-01
5 6 ← 4 5	443116.1690	(0100)	–0.0077	39.35	46.95	0.19E+00	0.35E-01
5 4/5 - 4 4/4	443117.0978	(0020)	–0.0015	—	0.30	—	0.22E-03
5 4 ← 4 4	443118.0588	(0040)	0.0041	1.33	0.05	0.63E-02	0.40E-04
6 ⟵ 5	531716.3488	(0024)					
6 6 ← 5 6	531714.6673	(0040)	0.0030	0.93	0.03	0.67E-02	0.45E-04
6 6/7 - 5 6/6	531715.5174	(0020)	–0.0024	—	0.47	—	0.83E-03
6 5 ← 5 4	531716.3479	(0100)	0.0437	27.22	22.27	0.20E+00	0.39E-01
6 6 ← 5 5	531716.3479	(0100)	–0.0018	32.44	31.64	0.24E+00	0.56E-01
6 7 ← 5 6	531716.3479	(0100)	–0.0273	38.49	44.54	0.28E+00	0.78E-01
6 5/6 - 5 5/5	531717.2804	(0020)	–0.0019	—	0.34	—	0.60E-03
6 5 ← 5 5	531718.2216	(0040)	0.0065	0.93	0.03	0.67E-02	0.45E-04
7 ⟵ 6	620303.9976	(0032)					
7 7 ← 6 7	620302.2905	(0040)	0.0029	0.68	0.01	0.69E-02	0.47E-04
7 7/8 - 6 7/7	620303.1550	(0020)	0.0016	—	0.42	—	0.14E-02
7 6 ← 6 5	620304.0022	(0100)	0.0377	28.21	23.85	0.28E+00	0.81E-01
7 7 ← 6 6	620304.0022	(0100)	0.0036	32.68	32.01	0.33E+00	0.11E+00
7 8 ← 6 7	620304.0022	(0100)	–0.0169	37.75	42.71	0.38E+00	0.14E+00
7 6/7 - 6 6/6	620304.9107	(0020)	–0.0035	—	0.33	—	0.11E-02
7 6 ← 6 6	620305.8325	(0040)	0.0027	0.68	0.01	0.69E-02	0.47E-04
8 ⟵ 7	708876.9976	(0043)					
8 8 ← 7 8	708875.2646	(0040)	–0.0028	0.52	0.01	0.67E-02	0.44E-04
8 8/9 - 7 8/8	708876.1421	(0020)	0.0007	—	0.36	—	0.20E-02
8 7 ← 7 6	708877.0051	(0100)	0.0334	28.90	24.99	0.37E+00	0.14E+00
8 8 ← 7 7	708877.0051	(0100)	0.0063	32.80	32.20	0.42E+00	0.18E+00
8 9 ← 7 8	708877.0051	(0100)	–0.0104	37.25	41.54	0.48E+00	0.23E+00
8 7/8 - 7 7/7	708877.8999	(0020)	–0.0010	—	0.31	—	0.17E-02
8 7 ← 7 7	708878.8067	(0040)	0.0037	0.52	0.01	0.67E-02	0.44E-04

Table 1 (continued).

J' F'' J'' F''	ν_{exp}	σ	Diff	$^{R}I_{lin}$	$^{R}I_{sat}$	$^{A}I_{lin}$	$^{A}I_{sat}$
9 ⟵ 8	797433.2575	(0057)					
9 8 ← 8 7	797433.2623	(0100)	0.0257	29.42	25.90	0.45E+00	0.20E+00
9 9 ← 8 8	797433.2623	(0100)	0.0035	32.91	32.39	0.50E+00	0.25E+00
9 10 ← 8 9	797433.2623	(0100)	–0.0103	36.85	40.61	0.56E+00	0.31E+00
10 ⟵ 9	885970.6863	(0076)					
10 9 ← 9 8	885970.6949	(0100)	0.0258	29.83	26.61	0.51E+00	0.26E+00
10 10 ← 9 9	885970.6949	(0100)	0.0071	32.99	32.56	0.56E+00	0.32E+00
10 11 ← 9 10	885970.6949	(0100)	–0.0041	36.51	39.86	0.62E+00	0.39E+00
11 ⟵ 10	974487.1938	(0099)					
11 10 ← 10 9	974487.1998	(0100)	0.0204	30.14	27.17	0.55E+00	0.30E+00
11 11 ← 10 10	974487.1998	(0100)	0.0044	33.06	32.68	0.60E+00	0.36E+00
11 12 ← 10 11	974487.1998	(0100)	–0.0045	36.25	39.30	0.66E+00	0.43E+00
12 ⟵ 11	1062980.6900	(0128)					
12 11 ← 11 10	1062980.6890	(0800)	0.0108	30.44	27.72	0.56E+00	0.32E+00
12 12 ← 11 11	1062980.6890	(0800)	–0.0028	33.09	32.75	0.61E+00	0.37E+00
12 13 ← 11 12	1062980.6890	(0800)	–0.0096	36.01	38.79	0.67E+00	0.44E+00
13 ⟵ 12	1151449.0860	(0163)					
13 12 ← 12 11	1151449.0880	(0800)	0.0116	30.67	28.14	0.55E+00	0.31E+00
13 13 ← 12 12	1151449.0880	(0800)	0.0000	33.11	32.80	0.60E+00	0.36E+00
13 14 ← 12 13	1151449.0880	(0800)	–0.0048	35.83	38.40	0.65E+00	0.42E+00
14 ⟵ 13	1239890.2936	(0206)					
14 13 ← 13 12	1239890.1680	(1000)	–0.1180	30.87	28.53	0.52E+00	0.27E+00
14 14 ← 13 13	1239890.1680	(1000)	–0.1277	33.18	32.95	0.56E+00	0.31E+00
14 15 ← 13 14	1239890.1680	(1000)	–0.1305	35.61	37.94	0.60E+00	0.36E+00
15 ⟵ 14	1328302.2252	(0258)					
15 14 ← 14 13	1328302.2010	(1500)	–0.0185	31.03	28.82	0.47E+00	0.22E+00
15 15 ← 14 14	1328302.2010	(1500)	–0.0264	33.19	32.98	0.51E+00	0.26E+00
15 16 ← 14 15	1328302.2010	(1500)	–0.0273	35.48	37.69	0.54E+00	0.29E+00
16 ⟵ 15	1416682.7942	(0320)					
16 15 ← 15 14	1416683.0380	(2000)	0.2477	31.17	29.09	0.42E+00	0.17E+00
16 16 ← 15 15	1416683.0380	(2000)	0.2414	33.20	32.99	0.44E+00	0.20E+00
16 17 ← 15 16	1416683.0380	(2000)	0.2424	35.37	37.45	0.47E+00	0.22E+00
17 ⟵ 16	1505029.9149	(0395)					
17 16 ← 16 15	1505030.1900	(2000)	0.2770	31.28	29.29	0.35E+00	0.12E+00
17 17 ← 16 16	1505030.1900	(2000)	0.2725	33.23	33.06	0.38E+00	0.14E+00
17 18 ← 16 17	1505030.1900	(2000)	0.2754	35.26	37.24	0.40E+00	0.16E+00
18 ⟵ 17	1593341.5028	(0484)					
18 17 ← 17 16	1593341.5360	(2000)	0.0333	31.39	29.50	0.29E+00	0.84E-01
18 18 ← 17 17	1593341.5360	(2000)	0.0305	33.23	33.07	0.31E+00	0.94E-01
18 19 ← 17 18	1593341.5360	(2000)	0.0354	35.18	37.06	0.32E+00	0.11E+00
21 ⟵ 20	1858042.2388	(0865)					
21 20 ← 20 19	1858042.2210	(0300)	–0.0234	31.63	29.97	0.13E+00	0.18E-01
21 21 ← 20 20	1858042.2210	(0300)	–0.0209	33.28	33.18	0.14E+00	0.20E-01
21 22 ← 20 21	1858042.2210	(0300)	–0.0097	34.94	36.56	0.15E+00	0.22E-01
22 ⟵ 21	1946190.8707	(1041)					
22 21 ← 21 20	1946190.8800	(0300)	0.0018	31.72	30.14	0.98E-01	0.96E-02
22 22 ← 21 21	1946190.8800	(0300)	0.0061	33.27	33.15	0.10E+00	0.11E-01
22 23 ← 21 22	1946190.8800	(0300)	0.0194	34.88	36.45	0.11E+00	0.12E-01

[a] ν_{exp} consist of two entries for each rotational transition: the first entry represents the calculated hyperfine-free rotational frequency, the other are measured hyperfine lines. For each transition the corresponding standard deviation (σ), a difference obs.-calc., relative (^{R}I) and absolute (^{A}I) intensities are given. Both intensities are listed for the linear as well as saturation experiment. It is to be noted that crossover dips do not exist in linear spectroscopy.

Table 2. High Precision Molecular Constants of $H^{12}C^{14}N$ for the Ground Vibrational State.

Parameter		Present work[a]	Saturation dip data[b]	De Lucia and Gordy [9]	Maki [19]
B_0	kHz	44 315 974.970 (156)	44 315 974.937 (192)	44 315 975.7 (4)	44 315 976.02 (2))
D_0	kHz	87.216 35 (169)	87.216 01 (194)	87.24 (6)	87.2205 (9)
H_0	Hz	0.086 96 (242)	0.088 4 (43)	—	0.0088 1 (6)
eQq	kHz	–4 709.03 (162)	–4 710.013 (22)	–4 709.1 (13)	—
eQq_J	Hz	0.244 (88)	0.313 (50)	—	—
C_N	kHz	10.09 (38)	10.33 (51)	10.4 (3)	—
C_{NJ}	mHz	–0.014 3 (86)	–0.022 2 (116)	—	—

[a] Transitions used in the fit are: the beam maser data from De Lucia and Gordy [9], the sub-millimeter data from Maiwald et al. [18], and the Lamb dip data presented here. [b] Transitions taken from the present saturation dip data only.

precision measurements to the following energy expression:

$$E(J,F) = E_{\text{rot}}(J) + E_{\text{quad}}(J,F) + E_{\text{spin-rot}}(J,F)$$

$$= \mathbf{B}J(J+1) - \mathbf{D}[J(J+1)]^2 + \mathbf{H}[J(J+1)]^3$$

$$- \mathbf{eQ}\cdot(\mathbf{q}_0 + \mathbf{q}_J)\left\{\frac{3}{4}C(C+1) - J(J+1)I_N(I_N+1)\right\}$$

$$\cdot [2I_N(2I_N-1)(2J-1)(2J+3)]^{-1}$$

$$+ [\mathbf{C}_N + \mathbf{C}_{NJ}J(J+1)]C/2, \qquad (5)$$

where $\mathbf{eQ}\cdot\mathbf{q}_0$ (respective $\mathbf{eQ}\cdot\mathbf{q}_J$) represents a product of the (nitrogen) nuclear quadrupole coupling constant with the electronic field gradient parameter (respectively its centrifugal distortion contribution), $\mathbf{C}_N$ and $\mathbf{C}_{NJ}$ is the nitrogen spin rotation coupling parameter and its centrifugal distortion correction term, and finally C is so called Casimir's function which takes form

$$C = F(F+1) - J(J+1) - I_N(I_N+1). \qquad (6)$$

In this global fit we used three sources of data: i) the present saturation dip measurements, ii) the measured molecular beam maser transition frequencies of De Lucia and Gordy [9], and iii) the Doppler-limited measurements up to 2 THz recently published by Maiwald et al. [18]. From the latter data we have taken only those which are not covered by the present saturation dip data set, i.e.all rotational transitions between 1 THz and 2 THz.

In addition, we have made use of a molecular beam electric resonance study of the $J = 1$ energy level by Ebenstein and Muenter [20]. From a total of nine allowed and recorded electric resonance transitions with $\Delta J = 0$ in the $J = 1$ energy level, they derive very precise hyperfine properties of the ground state level including the nuclear quadrupole coupling constant for $J = 1$:

eQq = –4 707.83(6) kHz,
Ebenstein and Muenter, 1984.

From the molecular beam maser transitions of the $J = 1 \rightarrow 0$ and $J = 2 \rightarrow 1$ transitions the nuclear quadrupole constant was derived to be

eQq = –4 709.1(13) kHz, De Lucia and Gordy, 1969.

From the present, rather extended saturation dip measurements together with the molecular maser beam data, we obtain from the global fit values for both, the electric nuclear quadrupole constant and the corresponding centrifugal distortion contribution:

eQq = –4 709. 03 (162) kHz (present work),
eQq_J = 0.244 (88) Hz (present work).

Comparison between the three results on the electrical quadrupole moment, eQq, shows that our newly derived value agrees with the De Lucia and Gordy value within their respective standard deviations. There exists a slight discrepancy of our eQq-value and the one quoted for the J = 1 energy levels by Ebenstein and Muenter [20], however still within their quoted standard deviations. We consider this small difference in our respective the eQq-values to arise as a consequence of its correlation with eQq_J parameter and neglecting of the hydrogen spin rotation and nuclear spin-spin interactions in our study.

Astrophysical Detection: HCN, $J = 4 \rightarrow 3$ and $3 \rightarrow 2$ Emission in TMC1

We report the detection of the two R branch transitions $J = 4 \rightarrow 3$ and $3 \rightarrow 2$ in the Taurus Molec-

ular Cloud 1, TMC1. The hyperfine splitting of the $J = 3 \rightarrow 2$ transition has been partially resolved, see Figure 5. Comparison with the laboratory spectrum shown in Fig. 2.1 helps to identify the two interstellar HCN emission features. Before we discuss the new HCN detection, we present a short overview of the unique interstellar cold cloud TMC1.

The distribution of interstellar and circumstellar HCN proves it to be an ubiquitous and abundant molecule with which the conditions in molecular clouds can be traced easily. Due to the high permanent electric dipole moment of 2.99 Debye in the vibrational ground state, HCN will be excited via collisions only in the denser regions of molecular clouds. Thus HCN serves as an important indicator for tracing a variety of different high density physical phenomena, which range from the denser cores of star forming regions and dense shells of circumstellar envelopes such as that of IRC10216 to proto-planetary nebulae like CRL618 [22].

Since the detection of HCN in interstellar space by the $J = 1 \rightarrow 0$ R branch transition at 88.6 GHz, it has become clear that the electric nuclear quadrupole splitting of the ^{14}N-nucleus can be resolved only for this transition in most interstellar sources. For the next three higher J transitions, i. e. J = 2-1, 3-2, and 4-3, the hyperfine splitting of the center components and the two outer $\Delta F = 0$ components can hopefully be detected in cold, dark, and quiescent interstellar clouds. This represents a special class of molecular clouds, which are fairly dense, but no star formation has started yet. The physical conditions of these cold condensations are characterized by kinetic temperatures of 10 K and volume densities in excess of 10^4 cm^{-3}. The Taurus Molecular Cloud region contains many smaller core regions, one of them is the somewhat unique source named TMC1. Is the chemistry in TMC1 unique?

In TMC-1 the fractional abundance of complex hydrocarbon species and their derivatives are greater than in any other known interstellar source. The long linear unsaturated nitriles known as *cyanopolyynes*, with formulas H(C≡C)$_n$-C≡N, n = 0-5, and other carbon chain species represent conspicuous eigensignatures of the source TMC1. Formally, one might consider HCN the shortest of the cyanoplyynes. In the light of molecules tracing high density, TMC-1 exhibits an elongated structure with molecular emission stretched out along a ridge of approximate dimension 0.06 × 0.6 pc^2. It resembles somewhat a "cigar in space". On an even smaller scale, TMC-1 exhibits two main emission peaks, known as the *cyanopolyyne* and *ammonia* peak. These are two abundance maxima, separated by about 0.3 pc.

The interstellar line-width in TMC1 is determined by the clouds kinetic temperature which is about 10 K, and the line-width equals the Doppler width $2(\Delta\nu)_d = 7.15\times10^{-7}$ (T/M)$^{1/2}\nu_0$ (see e. g. [1]). The linewidth (HPFW) in TMC1 is about 0.5 km/s,which is wider than the Doppler width of about 0.13 km/s. Therefore, the kinetic temperature is but one factor to determine the linewidth, but the turbulence even for TMC1 cannot be neglected entirely. As far as turbulence in molecular clouds is concerned, TMC-1 is thus a "calm" condensation without any known embedded star. Due to its small size, TMC-1 could hardly be detected were it at a significantly longer distance.

The observations were carried out with the 3 m sub-millimeter radio-telescope at KOSMA. The Cologne Observatory for Sub-Millimeter Astrophysics, KOSMA is the home of the Cologne 3 m submillimeter radio-telescope located on the Gornergrat (altitude 3100 m) near Zermatt in Switzerland. Both the HCN transitions, i. e. J = 3-2 and 4-3 lines, were detected in TMC1 at the cyanopolyyne peak. It might be mentioned in passing that the receivers installed at KOSMA employ exclusively SIS (Superconductor-Insulator-Superconductor) mixers which are designed and built in our Cologne Nano-Laboratories. Similarly, as backends we rely exclusively on acousto-optical spectrometers (AOS). For the HCN detection we used the 2000 channel Cologne-built high resolution AOS with a bandwidth of 59 MHz and appropriately a frequency resolution of 53 kHz.

In the case of evaluating the newly observed spectra, we measured the frequencies of the two hyperfine components of the J = 3-2 lines assuming the velocity of TMC1 as 5.85 km s^{-1} (velocity with respect to the local standard of rest) and obtained the following results for the rest frequencies of the J = 3-2 transition:

	Interstellar	Experimental Laboratory Data
J = 3-2: ΔF = 1:	265886.543 MHz	265886.397 MHz (ΔF = 1 Intensity weighted value)
J = 3-2: F = 3-3:	265884.851 MHz	265884.883 MHz
Freq. diff. $\Delta\nu$:	1.692 MHz	1.514 MHz

and for the rest frequency of the J = 4-3 transition:

	Interstellar	Experimental
J = 4-3; ΔF = 1:	3544505.467 MHz	354505.451 MHz (ΔF = 1 Intensity weighted value)

By taking into account the frequency resolution of the AOS, the latter two frequencies of the J = 3-2 and 4-3; ΔF = 1 transitions agree closely with the laboratory measured frequencies. However, in case of the J = 3-2, ΔF = 1 emission, the observed frequency difference between the two hyperfine components in TMC1 is by about 0.15 MHz higher than the laboratory value. This difference is probably due to self-absorption, a situation which often happens in sources with relatively strong interstellar emission. Absorption stems from the fact that the emitting region is often surrounded by colder material absorbing part of the line emission but at slightly different velocities.

Closer inspection of Fig. 5 reveals that the intensity relation of the two hyperfine components does not represent the intensity ratio expected for the condition of Local Thermodynamic Equilibrium. The J = 3-2 line displays for the ΔF = 1 component (overlap of F = 4-3, 3-2, 2-1) and for the F = 3-3 component nearly equal intensities. Theoretically, the ΔF = 1 component is much more intense than the F = 3-3 component. In addition, the F = 2-2 component is not detected, although the F = 3-3 and 2-2 components should exhibit the same intensity (see Table 1).

We performed model calculations to explain these abnormal intensities including hyperfine selective collisional excitation. As a result, the intensities could be roughly explained [22] (Takano, Stutzki, and Winnewisser 1999), and the HCN abundance and H_2 density could be obtained. Details of the calculations and the results will be published separately.

Conclusions

The present measurements provide ground state rotational transitions of HCN, all measured with sub-Doppler saturation spectroscopy. Commencing with the J = 3 ← 2 transition, all nine rotational transitions have been recorded in sub-Doppler resolution as high as J = 11 ← 10 just below 1 THz. We have portrayed these nine transitions in a special sequence of figures (Fig. 2.1-2.9) which are intended to allow detailed and scrutinizing checks of the Lamb-dip spectra and the occurrence of crossover dips. In addition, saturation spectroscopy in the terahertz region reveals detailed spectral features such as hyperfine structures, which otherwise would remain concealed within the Doppler widths.

The intensities of the observed saturation dips and crossover dips are found to be consistent with theory (see Table I). Nine consecutive rotational transitions with their associated hyperfine structure, which has partly been resolved, form this new data set. Together with the molecular beam maser measurements of the J = 1 → 0 and J = 2 → 1 transitions by De Lucia and Gordy this combined data set represents hitherto one of the very rare cases, for which all measurable R-branch transitions have been recorded in sub-Doppler resolution and with an absolute frequency accuracy for each line of typically ± 2 kHz or better. From these data, molecular constants for the ground state of HCN were determined. In fact, the quality of the Lamb-dip data demonstrates the importance of these measurements in better determining the constants for this well measured (in the infrared) molecule [19, 23].

This detailed study of the vibrational ground state rotational spectrum of $H^{12}C^{14}N$ has been extended towards its various isotopomers, notably $H^{13}C^{14}N$ and $D^{12}C^{14}N$. In addition, saturation dip spectroscopy has been used to check out various vibrational excited states. These results will be published in due course.

The detection of millimeter wave emission of HCN originating from the dark cloud TMC1 with the KOSMA 3 m Sub-Millimeter wave telescope suggests that it will be profitable to search for HCN with a larger aperture millimeter- / sub-millimeter telescope, like the 30 m IRAM telescope.

For conducting these detailed investigations of the laboratory and spectra of some very selected molecules, there exists, however, an underlying broader scope. Recently, we have measured and analysed in similarly scrutinizing detail, the rotational spectra of the six stable isotopomers of CO to the same level of detail [25 - 29]. We provide this way rotational spectra of spectroscopically important molecules recorded to a level of accuracy which corresponds to the state of the art and in a frequency domain around 1 THz not available in the past. As the data become available after passing scrutinizing checks, they will form part of the basis of the Cologne Database for Molecular Spectroscopy, CDMS, which can be accessed online free of charge via http://www.ph1.uni-koeln.de/vorhersagen/ or alternatively via the shortcut http://www.cdms.de [30].

Acknowledgements

The Cologne group has been supported by the Deutsche Forschungsgemeinschaft via research grants SFB-494. We much acknowledge the Ministry of Science of the Land Nordrhein-Westfalen / Germany for financial support. Stepan Urban acknowledges support through the Grant Agency of the Czech Republic (#203/01/1274). The collaborative work between the groups of Stepan Urban, Prague and the spectroscopy group in Cologne has been additionally supported by the International Office of the Federal Ministry of Education and Science at the DLR via grant CZE 00/030. The work carried out on the high power BWOs by ISTOK in collaboration with the Cologne group has been supported by the Deutsche Forschungsgemeinschaft through a grant aimed to support Eastern and Central European Countries and Republics of the Former SU. All support is greatly appreciated.

[1] A. G. Smith, W. Gordy, J. W. Simmons, and W. V. Smith, Phys. Rev. **75**, 260 (1949).
[2] J. W. Simmons, W. E. Anderson, and W. Gordy, Phys. Rev. **77**, 77 (1950); ibid, **86**, 1055 (1952).
[3] L.E. Snyder and D. Buhl, Astrophys. J. **163**, L47 (1971).
[4] R. Lucas and J. Cernicharo, Astron. & Astrophys. **218**, L20 (1989).
[5] J. Stutzki, R. Genzel, A. I. Harris, J. Herrman, and D. T. Jaffe, Astrophys. J. **330**, 129 (1988).
[6] P. Schilke, D. M. Mehringer, and K. M. Menten, Astrophys. J. **528**, L37 (2000).
[7] F. J. Lovas, J. Phys. Rev. Data **7**, 1445 (1978).
[8] J. Preusser and A. G. Maki, J. Mol. Spectrosc. **162**, 484 (1993).
[9] F. C. De Lucia and W. Gordy, Phys. Rev. **187**, 58 (1969).
[10] S. P. Belov, Th. Klaus, G. M. Plummer, R. Schieder, and G. Winnewisser, Z. Naturforsch. **51a**, 1187 (1995).
[11] G. Winnewisser, S. P. Belov, Th. Klaus, and Š. Urban, Z. Naturforsch. **51a**, 200 (1996).
[12] Th. Klaus, S. P. Belov, and G. Winnewisser, J. Mol. Spectrosc. **187**, 109 (1998).
[13] W. E. Lamb, Phys. Rev. **134**, 1429 (1964).
[14] T. Oka, Frontiers in Laser Spectroscopy (R. Balian, S. Haroche, and S. Lieberman, Eds.), pp. 531, North Holland, Amsterdam 1977.
[15] R. Karplus and J. Schwinger, Phys. Rev. **73**, 1020 (1948).
[16] G. Magerl, W. Schupita, J. M. Frye, W. A. Kreiner, and T. Oka, J. Mol. Spectrosc. **107**, 72 (1994).
[17] G. Winnewisser, Vib. Spectrosc. **8**, 241 (1995).
[18] F. Maiwald, F. Lewen, V. Ahrens, M. Beaky, R. Gendriesch, A. N. Koroliev, A. A. Negirev, D. G. Paveljev, B. Vowinkel, and G. Winnewisser, J. Mol. Spectrosc. **202**, 166 (2000).
[19] A. G. Maki, 2001, private communication.
[20] W. L. Ebenstein and J. S. Muenter, J. Chem. Phys. **80**, 3989 (1984).
[21] S. Thorwirth, F. Wyrowski, P. Schilke, K. M. Menten, S. Brünken, H. S. P. Müller, and G. Winnewisser, Astrophys. J., submitted for publication (2002).
[22] S. Takano, J. Stutzki, and G. Winnewisser, IAU symposium 197, (1999) Astrochemistry: from molecular clouds to planetary systems, p. 107.
[23] A. Maki, G. Ch. Mellau, S. Klee, M. Winnewisser, and W. Quapp, J. Mol. Spectrosc. **202**, 82 (2000).
[24] F. Lewen, R. Gendriesch, I. Pak, D. G. Paveliev, M. Hepp, R. Schieder, and G. Winnewisser, Rev. Sci. Instrum. **69**, 32 (1998).
[25] G. Winnewisser, S. P. Belov, Th. Klaus, and R. Schieder, J. Mol. Spectrosc. **184**, 468 (1997).
[26] G. Klapper, F. Lewen, R. Gendriesch, S.P. Belov, and G. Winnewisser, J. Mol. Spectrosc. **201**, 124 (2000).
[27] G. Klapper, F. Lewen, S. P. Belov, and G. Winnewisser, Z. Naturforsch. **55a**, 441 (2000).
[28] G. Klapper, F. Lewen, R. Gendriesch, S.P. Belov, and G. Winnewisser, Z. Naturforsch. **56a**, 329 (2001).
[29] G. Klapper, L. Surin, F. Lewen, I. Pak, and G. Winnewisser, Astrophys. J., in press 2002.
[30] H. S. P. Mueller, S. Thorwirth, D. D. Roth, and G. Winnewisser, Astron. & Astrophys. **370**, L49 (2001).